Journal of Catalysis 287 (2012) 138–148

Contents lists available at SciVerse ScienceDirect

Journal of Catalysis

journal homepage: www.elsevier.com/locate/jcat

# Photocatalytic oxidation of ethanol and isopropanol vapors on cadmium sulfide

Maxim A. Nasalevich, Ekaterina A. Kozlova, Tatyana P. Lyubina, Alexander V. Vorontsov *

*Boreskov Institute of Catalysis, Novosibirsk 630090, Russian Federation*
*Novosibirsk State University, Novosibirsk 630090, Russian Federation*

ARTICLE INFO

*Article history:*
Received 20 July 2011
Revised 13 December 2011
Accepted 16 December 2011
Available online 21 January 2012

*Keywords:*
Green chemistry
Solar light
Synthesis
Photocatalytic oxidation
Batch reactor
Flow-type reactor
Ethanol
Isopropanol
Photocorrosion
GC–MS

ABSTRACT

CdS-based catalysts preparation has been investigated, and the obtained photocatalysts were characterized and tested in photocatalytic oxidation of ethanol and isopropanol vapors under visible light irradiation ($\lambda > 420$ nm) with oxygen of air. The catalysts were prepared with a two-step method: (1) reaction between $CdCl_2$ and NaOH and (2) exchange of hydroxide ions of $Cd(OH)_2$ intermediate with $S^{2-}$ to form CdS. Influence of the reagents addition rate, stirring rate, temperature of the reaction mixture and the reagents' ratio on the oxidation rate of alcohols on solids was investigated. It was found that the rate of photooxidation increases with the increase in the stirring rate and with the decrease in the reagents addition rate during the synthesis. The photocatalytic activity as a function of sulfur content reaches the highest value for the stoichiometric CdS, which is obtained at $\geqslant$2:1 $S^{2-}$ to $Cd^{2+}$ molar ratio in precursors. Kinetic features of the isopropanol photocatalytic oxidation were studied. The Langmuir–Hinshelwood model describes satisfactorily the rate vs. concentration curve. The increase in the air relative humidity results in higher isopropanol oxidation rate. Partial deactivation of CdS catalyst was observed and described with exponential decay. Deactivation was less pronounced at high relative humidity. CdS deactivation took place due to the surface sulfur ions oxidation with formation of $SO_4^{2-}$ groups. The results show a potential of CdS photocatalysis for solar light–driven green oxidation processes of organic compounds.



## 1. Introduction

The growing concerns about the environmental issues and the exhaustion of natural resources have resulted in the development of green and sustainable methods for chemical transformations of organic compounds. Solar light represents a renewable energy source that can be used for driving various chemical transformations. However, direct photochemical transformations of organic compounds upon absorption of solar light are often obstructed by the low absorption of reagents in the visible light region. Application of suitable photocatalyst that absorbs wider spectrum of light could lead to visible light reaction initiation and increased selectivity toward desirable products.

Photocatalytic processes have already been used for selective oxidation [1,2], condensation [3], isomerization [4], $CO_2$ reduction [5,6], hydrogenation [7], hydrogen production [8] and other organic reactions. Titanium dioxide is often used for photocatalytic reactions as highly active catalyst. In relation to oxidative reactions, $TiO_2$ main disadvantages are low selectivity toward partial oxidation in aerobic conditions (e.g. oxidation of aryl alcohols [9]) and wide band gap of about 3 eV that causes UV light absorption only. Other active semiconductor photocatalysts such as ZnO and ZnS also absorb UV light only [10–13]. Cadmium sulfide, on the contrary, is capable of driving partial oxidation with high selectivity and has band gap for bulk material of about 2.4 eV that corresponds to the absorption of light at $\lambda < 515$ nm [14–17]. Under illumination with visible light ($\lambda > 400$ nm), CdS was proven to be one of the most active photocatalysts [18]. Various organic reactions like hydrogen generation [19,20], oxidation of dyes and simpler organics [21–25], condensation of amines and alcohols [26], racemization and cyclization of aminoacids [27,28], reduction of nitrobenzene [29] have already been carried out successfully over CdS in liquid phase using visible light in many cases.

Performing photocatalytic oxidation in gas phase has proven to be advantageous since the rates are much higher due to the availability of oxygen, absence of solvent adsorption competition and enhanced mass transport. The gas-phase reactions over CdS reported so far are limited to few examples [30,31], and to the best of our knowledge, no reports are available for oxidation.

The CdS photocatalyst properties depend on composition, phase and morphology. The composition is determined by CdS preparation that is mainly performed via reaction of $Cd^{2+}$ and $S^{2-}$ ions in solution. The sulfide ions can be added as is, or they can be generated *in situ* by hydrolysis of thiourea ($NH_2CSNH_2$), as realized in thermohydrolysis [22] and chemical bath deposition [31], or can be obtained from elemental sulfur by dark or photocatalytic

* Corresponding author. Fax: +7 383 3331617.
*E-mail address:* voronts@catalysis.ru (A.V. Vorontsov).

0021-9517/$ - see front matter © 2011 Elsevier Inc. All rights reserved.
doi:10.1016/j.jcat.2011.12.014

reduction with sacrificial agents [32]. $Cd(OH)_2$ and CdO can serve as Cd source for CdS synthesis via anion-exchange mechanism [20].

CdS has two main crystallographic modifications – more stable hexagonal (wurtzite type) and cubic (sphalerite type), both being used as photocatalysts with similar properties, and both hexagonal and cubic [33] phase possesses high photocatalytic activity [20,34,35].

The morphology of CdS is controlled during synthesis, so that different particle shapes like nanowires, nanoribbons, hollow particles, etc. can be obtained [36,37]. The porous structure can be controlled by applying templates (structure directing agents) like polystyrene latex particles [21] and bio-organic matrixes [23]. Alternatively, the pores are formed during CdS synthesis from $Cd(OH)_2$ precursor since the molar volume of CdS is smaller than that of $Cd(OH)_2$ [20].

In the present work, we focused on the optimization of CdS preparation using the self-templated two-step synthesis with $Cd(OH)_2$ intermediate. The CdS catalysts were evaluated in partial oxidation of ethanol and isopropanol vapors with oxygen of air under visible light. A very high selectivity to acetaldehyde and acetone was obtained. The highest activity was attained for CdS synthesized at definite $Cd^{2+}$ and $S^{2-}$ precursor ratio, reagents addition rates and stirring conditions. Kinetic studies of ethanol and isopropanol oxidation revealed that Langmuir–Hinshelwood equation can be used to describe the substrate concentration effect. Partial deactivation of CdS was observed which is reduced at higher humidity. The oxidation of surface $S^{2-}$ into sulfate was determined to contribute to the CdS deactivation. Since the deactivation was incomplete, the process has prospects for green partial oxidation of alcohols with atmospheric oxygen.

## 2. Experimental

### 2.1. Reagents

$Na_2S{\cdot}xH_2O$ (32–38% (RT)) was a Fluka product, cadmium chloride and sodium hydroxide were purchased from Reakhim (Russia), and their purity was not less than 97–98%. Ethanol and isopropanol were purchased from Reakhim (Russia), and their purity was not less than 97–98%.

### 2.2. Preparation of catalysts

The synthesis of CdS was carried out according to the method proposed by Bao et al. [20]. It goes through the following two stages.

$$CdCl_2 + 2NaOH \rightarrow Cd(OH)_2 + 2NaCl, \quad (1)$$

$$Cd(OH)_2 + Na_2S \rightarrow CdS + 2NaOH. \quad (2)$$

A typical procedure was as follows. 100 ml of 0.1 M NaOH was taken in a 250-ml glass beaker; then, 10 ml of 0.1 M $CdCl_2{\cdot}2.5H_2O$ was slowly added to the above solution through a dropping funnel under stirring during 5 min. Magnetic stirrer was used to carry out convection. Additional measurements of shear stress and stirring energy were not performed, thus detailed parameters of stirring equipment are listed below. The tank had cylindrical shape (diameter 55 mm, height 120 mm) with no baffles, and the stir bar was 6 mm in diameter and 25 mm in length. The stirrer bar rotation velocity was varied from 26.16 to 125.57 rad/s, and the exact value is indicated in the text, tables and figures' captions. A white precipitate of cadmium hydroxide was obtained. Then, a proper amount of 0.1 M $Na_2S$·aqueous solution was added at the same stir bar rate to obtain a yellow-orange precipitate of CdS. Molar ratio of $S^{2-}$ to $Cd^{2+}$ varied from 0.26 to 6.24. The solution was centrifuged, and the resulting precipitate was washed thoroughly with distilled water 10–15 times. The precipitate was dried at 343 K overnight in an oven.

### 2.3. Catalyst characterization

Crystallographic structure of catalysts with different S to Cd ratio was investigated with X-ray diffraction technique (XRD). The XRD patterns were obtained by means of an X-ray diffractometer X'tra (Thermo, Switzerland) with a Cu K$\alpha$ source. Measurements were carried out from 20° to 65° of $2\Theta$ angle value with 0.05° increment and a point signal accumulation time 3 s.

The surface chemical composition and the sulfur electronic state in the fresh and deactivated CdS catalysts were examined with X-ray photoelectron spectroscopy (XPS). The XPS analyses were carried out on a SPECS' photoelectron spectrometer equipped with a hemispherical electron energy analyzer PHOIBOS-150 as reported in [38]. The core-level spectra were obtained using non-monochromatic Mg K$\alpha$ radiation ($h\nu$ = 1486.7 eV). All binding energies were referenced to the C1s peak at 284.8 eV, which corresponds to hydrocarbon impurities.

The surface morphology research by high-resolution transmission electron microscopy (HRTEM) was performed on a JEM-2010 electron microscope (JEOL, Japan) at the accelerating voltage of 200 kV and a lattice resolution of 0.14 nm.

The elemental analysis was made with X-ray fluorescence spectroscopy (XRF). XRF measurements were done with X-ray fluorescence spectrometer ARL ADVANT'X 3.6 kW. An X-ray tube with a rhodium anode was used as a radiation source (voltage 50 kV, current 40 mA). The samples were put into a cartridge that was covered with spectrolene six film. Data processing was made with QuantAS program.

The diffuse reflectance spectra recording was performed on Perkin Elmer UV/VIS spectrometer Lambda 35 with the integrating sphere RSA-PE-20 (Labsphere, USA) in the wavelength range between 200 and 1100 nm. Magnesium oxide was used as the reference material, assuming its reflectance equal to 100%.

### 2.4. Catalytic activity measurements

Photocatalytic activity measurements in the oxidation of the ethanol and isopropanol vapor were done in a batch and a flow reactor, respectively. The batch reactor consists of a 280-ml flask with a light source over it. The flask was irradiated by the light of a high-pressure mercury lamp «DRSh-1000» (1000 W, Russia) using a cutoff filter ($\lambda \geqslant 410$ nm). The intensity of the incident radiation was 166.5 W/m$^2$. The reaction was carried out under continuous magnetic stirring with the rate 600 rpm. The initial concentration of ethanol vapors was 607 ppm. The humidity of the air mixture was 60% at 25 °C. The photocatalyst (10 mg) was deposited on a glass slide; the area of the catalyst spot was 2 cm$^2$. Acetaldehyde was detected with a gas-chromatograph HP 5890. Oxidation was carried out at the temperature 25 °C.

The flow-type reaction setup was described earlier [38]. It consists of a thermostated stainless steel reactor with a quartz window at the top, air dosage blocks, air purification block, saturators, syringe pump for reagents addition, a gas-chromatograph equipped with a mass-selective detector and a PLOT Fused Silica column (25 m × 0.32 mm) coated with CP Poraplot QHT and data collection PC. A halogen lamp IEK (150 W) with a cutoff filter ($\lambda \geqslant 410$ nm) was used as a visible light source. The intensity of the incident radiation was 4.44 W/m$^2$. The gas mixture flow rate was about 17 ml/min. Isopropyl alcohol was injected into the air flow by means of the syringe pump with the rate 1.6 μl/h; this rate corresponds to the isopropanol concentration of 500 ppm in the inlet air flow. The humidity of the gas mixture was 65% unless

otherwise stated. Measurements of the relative humidity were performed at 25 °C. The reactor was thermostated at 40 °C. Photocatalyst (30 mg) was deposited on a glass slide; the area of the catalyst spot was 2.5 × 2.5 cm. Acetone and isopropanol were detected with GCMS. Since the CdS photocatalysts undergo partial deactivation during photocatalytic oxidation, the rate of oxidation was extrapolated to reaction beginning using the first five measurement points that corresponded to the first 70 min of reaction.

## 3. Results and discussion

The present study is focused on the preparation of active CdS photocatalysts, their characterization and investigation of kinetic features of alcohols oxidation by oxygen of air under visible light irradiation in the gas phase. While preparing series of CdS samples by the two-step $Cd(OH)_2$ precipitation and ion-exchange method, the following parameters were changed:

- $CdCl_2$ and $Na_2S$ solutions addition rate;
- stirring rate during precipitation and ion exchange;
- temperature;
- $Cd^{2+}$ to $S^{2-}$ molar ratio.

The next sections describe the characterization of obtained CdS samples, their activity in ethanol and isopropanol gas-phase photocatalytic oxidation and kinetics of oxidation and catalyst deactivation.

### 3.1. Catalysts characterization

The XRD patterns of CdS catalyst series with various stirring rate and reagent addition rate during their synthesis are demonstrated in Fig. 1. Intensive CdS peaks are observed at $2\theta = 26.5°$, 43.8° and 52°. The patterns can be attributed to hexagonal (wurtzite like) structure called Greenockite with stacking faults. About every three layers of the CdS wurtzite structure, there is a stacking defect as it was determined using XRD spectra modeling program described by Cherepanova and Tsybulya [39]. Therefore, the crystal structure can be considered as intermediate between hexagonal (wurtzite) and cubic (sphalerite). The presence of CdS hexagonal phase is in a good accordance with the previous data [20].

Coherent domain sizes were estimated to change from 5.0 to 6.4 nm when the stirring rate increased from 250 to 1000 rpm. Thus, the stirring rate has small effect on domain sizes. The coherent domain size increases from 7.1 to 9.1 nm when the reagents addition rate increases from 5 to 41.0 ml/min.

Since the S to Cd ratio has a large effect on photocatalytic activity, the catalysts prepared with different S to Cd ratio in the precursor solutions were subjected to detailed characterization. Table 1 demonstrates the results of their elemental analysis.

One can see that the catalyst samples contain impurities Cl, Al and Si with overall content below 3.27 wt.%. The principal impurity is Si at low S/Cd ratio, while at the higher ratio, it is Cl that gives the largest contamination. The Si contamination can be due to the glassware dissolution at high pH by NaOH. The elements O, H and C were not determined by the method used, but it is implied that the catalysts contain amorphous $Cd(OH)_2$ and $CdCO_3$ especially at the low S/Cd ratio. The content of these impurity phases decreases as the sulfur to cadmium ratio in the precursor solutions increases.

The morphology and the structure of the catalyst with the highest sulfur content were explored with HRTEM. The TEM images of catalyst #23 with different magnification are shown in Fig. 2.

This catalyst obtained with 2 to 1 S to Cd molar ratio in the synthesis is composed from small well-crystallized particles. These particles have many randomly arranged crystal lattices. The plane distances (*d*-values) at the different spots were found to be 3.59, 3.36, 3.16, 2.45, 2.07 and 1.90 Å representing the (100), (002), (101), (102), (110) and (103) lattice planes distance of hexagonal phase CdS (Greenockite structure) [40]. The shape and size of the obtained CdS nanostructures are very close to those of the $Cd(OH)_2$ intermediates [20]. Fig. 2A is a review image of CdS sample in the large (200 nm) scale and shows that the CdS particles form agglomerates of size above 100 nm. Fig. 2B shows a fragment of CdS with 50 nm scale in which a hollow flattened nanorod with the diameter about 50 nm and the wall thickness about 5 nm is present. Fig. 2C shows CdS nanoparticle in 10 nm scale. One can see that coherently scattering domains are about 2–5 nm in size.

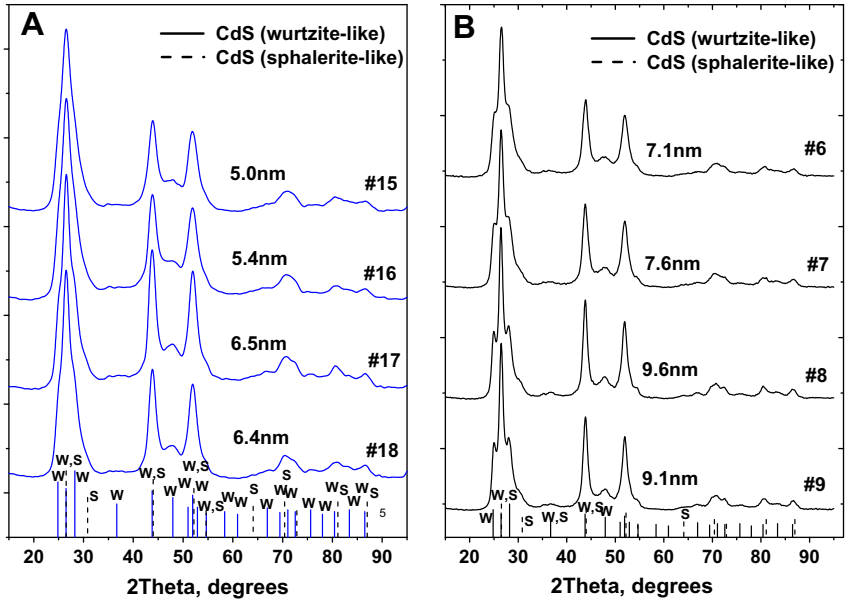


**Fig. 1.** XRD patterns of catalysts with different stirring rate (A) and reagent addition rate (B) in a range of 250–1000 rpm and 5–41 ml/min during the synthesis. The samples were obtained with 2-fold excess of sulfide ions to cadmium ions. The numbers above the curves denote crystallite size and catalyst number; the "W" and "S" denote wurtzite and sphalerite lines, respectively.

**Table 1**
Elemental analysis of catalysts series with various $S^{2-}$ to $Cd^{2+}$ ratio in the precursor solutions.

| $S^{2-}$ to $Cd^{2+}$ ratio | Element content (wt.%) | | | | |
|---|---|---|---|---|---|
| | Cd | S | Cl | Al | Si |
| 0.26 | 94.4 | 2.3 | 0.7 | 0.11 | 2.46 |
| 0.52 | 92.9 | 4.3 | 0.6 | 0.07 | 2.16 |
| 1 | 89.5 | 8.2 | 0.3 | 0.14 | 1.75 |
| 1.56 | 86.3 | 12.3 | 0.3 | 0.12 | 1.10 |
| 2.08 | 79.4 | 20.3 | 0.2 | 0.08 | 0.10 |
| 3.12 | 82.3 | 17.4 | 0.2 | 0.04 | 0.07 |
| 4.16 | 81.6 | 18.0 | 0.3 | 0.03 | 0.04 |
| 6.24 | 80.1 | 19.6 | 0.2 | 0.05 | 0.02 |

Energy-dispersive X-ray spectroscopy data confirm the presence of sulfur and cadmium in the specimen. In Fig. 2D, one can see several walls of the nanorods. Formation of these nanostructures is explained by the two-step synthesis scheme with $Cd(OH)_2$ intermediate. In contrast to the material described by Bao et al. [20], the amount of hollow nanorods in our sample is small that can be caused by the change of $Na_2S$ amount during the synthesis.

XRF measurements of the samples with different sulfur to cadmium ratio in the precursor solutions were made in order to estimate the catalyst elemental composition. As shown in Fig. 3, the sulfur to cadmium molar ratio in the catalysts depends strongly on the reagents solutions molar ratio used for CdS synthesis. This dependence is close to linear in the initial spot of the curves; the sulfur to cadmium ratio reaches its maximum value at 2:1 S to Cd molar ratio in the precursor solutions. Further increase in the reagents ratio during the synthesis does not yield the sulfur content growth. Moreover, sulfur to cadmium ratio in the catalyst decreases slightly when S to Cd molar ratio in solutions increases from 2 to 6.24. This decrease is, however, within the error of measurements (about 8% for the highest S to Cd ratio). Thus, it is established that the 2-fold excess of $Na_2S$ during the synthesis is required for the formation of nearly stoichiometric CdS.

Diffuse reflectance spectra of samples with various sulfur to cadmium molar ratio in synthesis were measured in order to determine the light absorption edges of catalysts. Fig. 4A exhibits absorption spectra of CdS catalysts. One can see that increase in sulfur content in catalysts in the series from #19 to #26 results in red shift of absorption threshold. The overall shift span is nearly 40 nm, and the largest change occurs from catalyst #21 to #22, which corresponds to attaining stoichiometric composition.

The Tauc's function was used to calculate the absorption edges of catalysts [41] as shown in Fig. 4B. Linear approximation of the Tauc's plots of $F(R)^2(h\nu)^2$ vs. $h\nu$ gives the absorption edges for catalysts: 490.12 (#19), 497.59 (#20), 500.20 (#21) 500.00 (#22) 529.24 (#23), 528.78 (#24), 529.46 (#25) and 532.19 (#26) nm, which correspond to 2.53, 2.49, 2.48, 2.48, 2.34, 2.35, 2.34 and 2.33 eV band gap values.

The observed shift of absorption edge is probably associated with the quantum-size effect [42]. The sizes of the particles can be estimated according to the band gap dependence of CdS particles size using the following equation [43].

$$R = \sqrt{\frac{2h\pi^2 \cdot E_g}{((E_g(R))^2 - E_g^2) \cdot m_e}}, \quad (3)$$

where $R$ – the particle radius, $E_g$ – the bulk semiconductor band gap energy, $E_g(R)$ – measured band gap and $m_e$ – the electron mass. The particle radii determined using the above expression were found to be 10.2, 11.0, 11.4, 11.3, 18.7, 18.5, 18.8 and 20.4 nm. The sizes are considerably larger than the coherent crystallite sizes from HRTEM (Fig. 2) data. This difference could be caused by electrons delocalization among the adjacent CdS crystallites that are tightly connected but are not coherently aligned though this issue has not been studied in detail. Indeed, Fig. 2 shows that the individual crystallites are fused into particles with sizes above 10 nm.

### 3.2. Influence of the catalysts synthesis conditions on the photocatalytic activity

In this work, four different series of catalysts were examined. Each series has one variable parameter of synthesis, while the three others are fixed. These parameters are stirring rate, reagents addition rate, synthesis temperature and sulfur to cadmium ratio in the precursor solutions. Oxidation of ethanol and isopropanol vapors was taken as the test reaction with formation of acetaldehyde and acetone, respectively, according to the next equations.

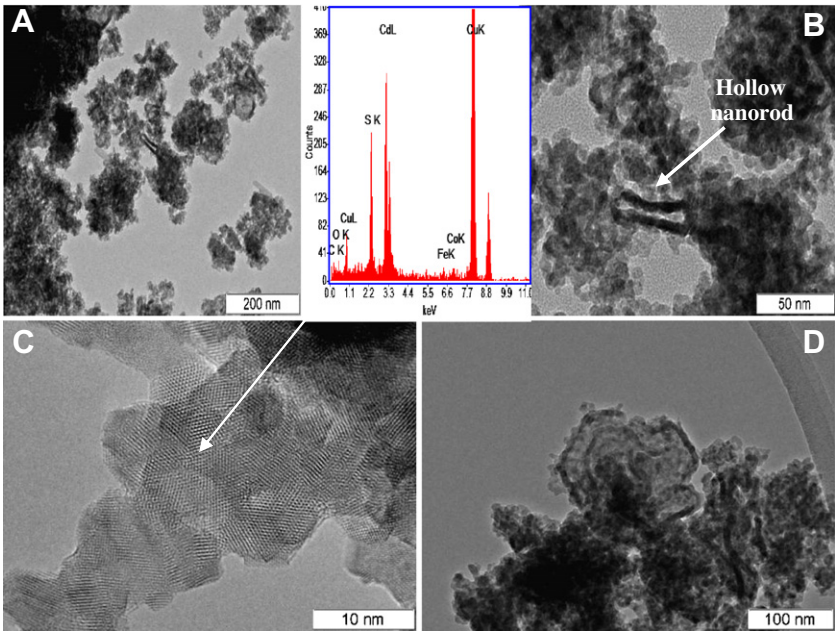


**Fig. 2.** HRTEM and TEM images and EDX data of catalyst #23.

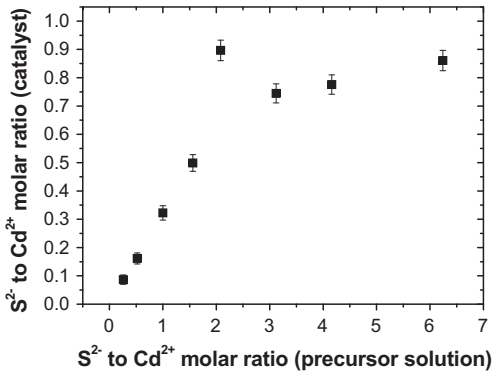


**Fig. 3.** Influence of Cd to S molar ratio in the precursor solutions on the sulfur to cadmium molar ratio in solids obtained as measured by XRF.

$$2C_2H_5OH + O_2 + 2h\nu \xrightarrow{CdS} 2CH_3CHO + 2H_2O, \quad (4)$$

$$2(CH_3)_2CHOH + O_2 + 2h\nu \xrightarrow{CdS} 2(CH_3)_2CO + 2H_2O. \quad (5)$$

Only acetaldehyde and acetone were detected in the gas-phase products during the alcohols oxidation over CdS samples. Therefore, the selectivity toward gaseous carbonyl compounds is high. Table 2 presents the rate of products formation over CdS photocatalysts synthesized at varied conditions.

The variation of the synthesis temperature from 25 to 70 °C resulted in negligible changes of the activity, and the corresponding results are not included in Table 2. The rate of stirring during the reagents mixing and further catalyst formation exerts significant influence on alcohols oxidation. Fig. 5A shows that the rate of acetaldehyde formation decreases linearly with an increase in reagents addition rate in the both stages of CdS preparation and attains the highest value at addition rate below 10 ml $min^{-1}$. A similar dependence was observed on the catalysts prepared with optimized S/Cd molar ratio in the isopropanol vapor photocatalytic oxidation. Fig. 5B indicates that the rate of acetone formation increases toward lower reagents addition rate. One can see that the rate is higher over optimized CdS photocatalysts significantly. Fig. 1B shows that the size of CdS coherent crystallite domains increases with an increase in reagents addition rate for samples 6–9. It is possible that the larger CdS crystallites possess smaller photocatalytic activity due to smaller surface area. The larger crystallites can be formed due to the higher rate of CdS formation at the higher rate of reagents addition.

Fig. 6 shows the influence of the stirring rate during the both stages of CdS preparation on the rate of ethanol (Fig. 6A) and isopropanol (Fig. 6B) vapors photocatalytic oxidation. One can see that the oxidation rate increases with an increase in the stirring rate and reaches a constant value for stirring at >1000 rpm.

The effect of the stirring rate is possibly not associated with the change in the CdS crystallite size since the increase in the stirring rate results in larger crystallites (Fig. 1).

The most intriguing series of CdS photocatalysts was obtained with the different S/Cd ratio in precursor solution. Eight samples with the S to Cd molar ratio during the synthesis from 0.26 to 6.24 were prepared. Fig. 7 demonstrates the dependence of rate of isopropanol vapors visible light oxidation on the S/Cd ratio in the precursor solutions. One can see that photocatalytic activity generally increases with the S/Cd ratio. The maximum activity was obtained on catalyst with the 2:1 sulfur to cadmium molar ratio. The influence of S to Cd ratio on photocatalytic activity has been investigated previously for CdS–$TiO_2$ thin-film catalysts. It was shown previously that the activity of $TiO_2$–CdS in the methanol vapors photocatalytic oxidation grows with the S:Cd ratio and

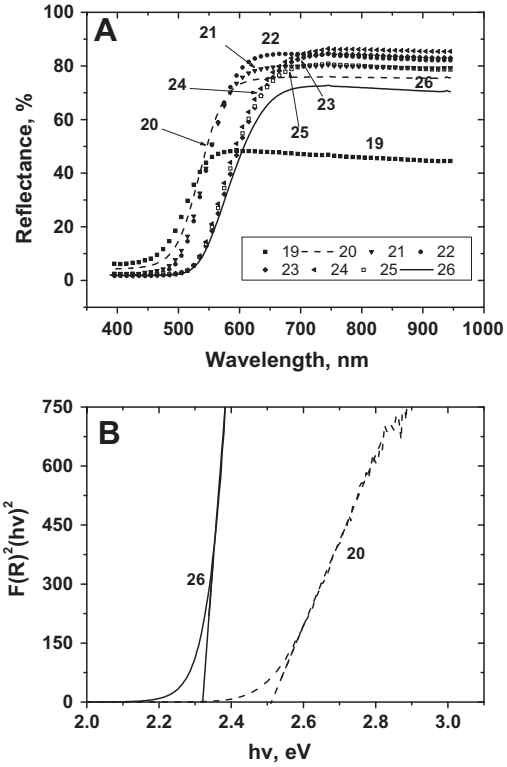


**Fig. 4.** Diffuse reflectance spectra of catalysts with different S to Cd molar ratio in the precursor solutions (A) and the Tauc's plot for band gap energy determination (B).

reaches its maximum value at 4:1 ratio for thin-film photocatalyst prepared by chemical bath deposition [31]. The highest activity for this ratio was explained by the highest crystallinity of the CdS film. This can also be the explanation for our study results. Indeed, the 2:1 ratio results in the formation of stoichiometric CdS catalysts with the minimum content of impurities (Fig. 3). Since impurities are often causing recombination of photogenerated charges and decrease in adsorption constant, their minimum content is essential for activity.

The impact of the catalysts stoichiometry becomes evident if the activity is plotted against the actual sulfur content according to data of Fig. 3 that were obtained from XRF. Fig. 8 shows that the acetone formation rate grows in a linear manner with the increase in sulfur content. Some decrease in activity for samples obtained at S/Cd ratio in excess of 2:1 can be associated with the sodium contamination of CdS due to the higher content of Na in solution the ion-exchange step of CdS preparation.

It is interesting to note that the photocatalytic activity does not decrease to zero if one extrapolates the linear dependence of activity on zero sulfur content. Since the $Cd(OH)_2$ formed without sulfide addition does not absorb visible light, its activity is assumed to be absent. Therefore, the dependence of activity on S/Cd ratio should change its shape at low values.

Since the content of the supposed active-phase CdS is different in different catalyst samples, Fig. 8 shows the rate of oxidation normalized to CdS content as well. One can see that the normalized rate decreases with an increase in sulfur content. This is a usual tendency in photocatalysis that an increase in the thickness of the catalyst layer absorbing light does not lead to continuous increase in the reaction rate. The fraction of light absorbed by photocatalyst obeys Bouger–Lambert exponential law. As will be shown lower, the rate obeys Langmuir–Hinshelwood equation and the combined effect of catalyst content and the reagents concentration can be expressed as follows.

**Table 2**
Influence of synthesis conditions on catalysts activity in photocatalytic oxidation of alcohol vapors. The catalysts were prepared at 25 °C. Catalytic activity test conditions: isopropanol initial concentration 500 ppm, relative humidity 65%.

| # | Reagents addition rate (ml/min) | Stirring rate (rpm) | $S^{2-}/Cd^{2+}$ ratio | $r$ (mol $(CH_3COH)$ $s^{-1}$ $cm^{-2}$ × $10^{11}$) | $r$ (mol $(CH_3)_2CO$) $s^{-1}$ $cm^{-2}$ × $10^{-11}$) | Quantum efficiency (%) |
|---|---|---|---|---|---|---|
| 1 | 1.88 | 750 | 0.26 | 3.93 | – | 0.06 |
| 2 | 3.64 | 750 | 0.26 | 3.75 | – | 0.05 |
| 3 | 8.6 | 750 | 0.26 | 3.97 | – | 0.06 |
| 4 | 14.3 | 750 | 0.26 | 3.03 | – | 0.04 |
| 5 | 54.5 | 750 | 0.26 | 2.4 | – | 0.04 |
| 6 | 5 | 1000 | 2 | – | 10.9 | 5.27 |
| 7 | 10 | 1000 | 2 | – | 10.1 | 4.89 |
| 8 | 25 | 1000 | 2 | – | 1.12 | 0.54 |
| 9 | 41 | 1000 | 2 | – | 0.8 | 0.38 |
| 10 | 8.0 | 250 | 0.26 | 1.87 | – | 0.03 |
| 11 | 8.0 | 500 | 0.26 | 2.42 | – | 0.04 |
| 12 | 8.0 | 750 | 0.26 | 3.58 | – | 0.05 |
| 13 | 8.0 | 1000 | 0.26 | 6.1 | – | 0.09 |
| 14 | 8.3 | 1200 | 0.26 | 6.19 | – | 0.09 |
| 15 | 7.0 | 250 | 2 | – | 4.55 | 2.20 |
| 16 | 7.0 | 500 | 2 | – | 6.45 | 3.12 |
| 17 | 7.0 | 750 | 2 | – | 8.84 | 4.28 |
| 18 | 7.0 | 1000 | 2 | – | 9.68 | 4.69 |
| 19 | 8.0 | 1200 | 0.26 | – | 2.94 | 1.54 |
| 20 | 8.0 | 1200 | 0.52 | – | 2.03 | 1.05 |
| 21 | 8.0 | 1200 | 1 | – | 3.42 | 1.76 |
| 22 | 8.0 | 1200 | 1.56 | – | 4.92 | 2.53 |
| 23 | 8.0 | 1200 | 2.08 | – | 5.31 | 2.58 |
| 24 | 8.0 | 1200 | 3.12 | – | 4.90 | 2.38 |
| 25 | 8.0 | 1200 | 4.16 | – | 4.88 | 2.37 |
| 26 | 8.0 | 1200 | 6.24 | – | 4.78 | 2.31 |

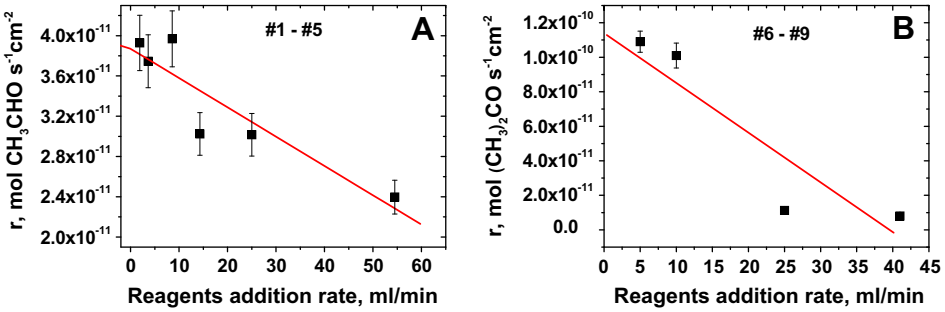


**Fig. 5.** Influence of reagents addition rate in CdS synthesis on acetaldehyde formation rate (A) and acetone formation rate (B) over obtained catalysts (see Table 2) in the photocatalytic oxidation of ethanol and isopropanol vapors, respectively. Ethanol initial concentration 607 ppm, reaction temperature 25 °C, isopropanol initial concentration 500 ppm, reaction temperature 40 °C, relative humidity 60% in both cases. #1–5 catalysts were synthesized at 750 rpm, while #6–9 at 1000 rpm.

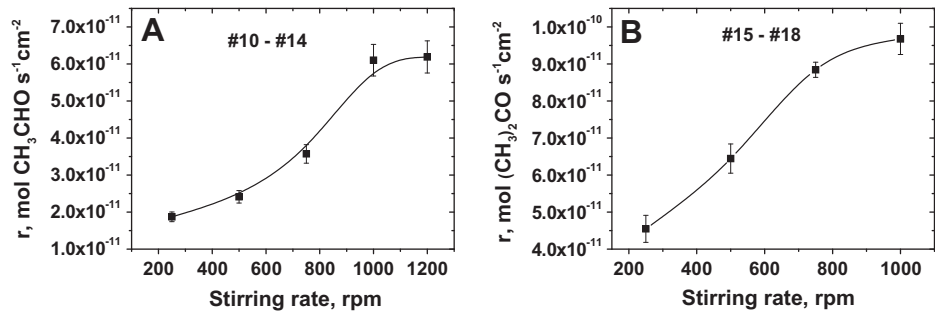


**Fig. 6.** Acetaldehyde formation rate (A) and acetone formation rate (B) in photocatalytic oxidation of ethanol and isopropanol vapors respectively, as a function of stirring rate during catalysts synthesis reaction. Numbers indicate catalysts being used (see Table 2). Ethanol initial concentration 607 ppm, reaction temperature 25 °C, isopropanol initial concentration 500 ppm, reaction temperature 40 °C, relative humidity 60% in both cases.

$$r = I_0\left(1 - 10^{-\frac{\alpha m \chi_S}{dS}}\right) \cdot \mathrm{LH}, \tag{6}$$

where $I_0$ is the incident photon irradiance (mol $s^{-1}$ $cm^{-2}$), $\alpha$ – CdS absorption coefficient ($\alpha \sim 4 \times 10^4$ $cm^{-1}$ at 500 nm [44]), $m$ – deposited photocatalyst mass (0.03 g), $\chi_S$ – sulfur mass fraction (dimensionless), $d$ – catalyst density (~4 g $cm^{-3}$), $S$ – geometric area of photocatalyst spot (6.25 $cm^2$) and LH – Langmuir–Hinshelwood dependence of the rate on concentrations (dimensionless, see Eq.

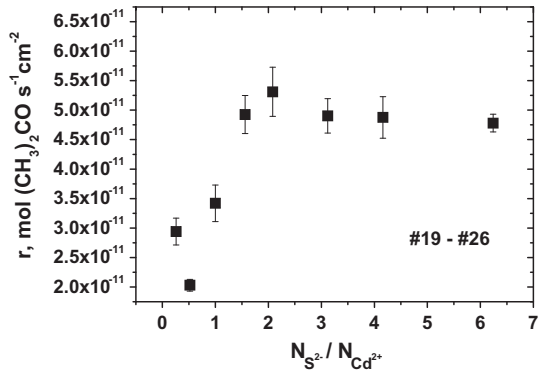


**Fig. 7.** Dependence of acetone formation rate in isopropanol vapors photocatalytic oxidation on ratio of sulfur and cadmium in the precursor solutions. $r$ is the initial acetone formation rate. Isopropanol initial concentration 500 ppm, relative humidity 65%, reaction temperature 40 °C.

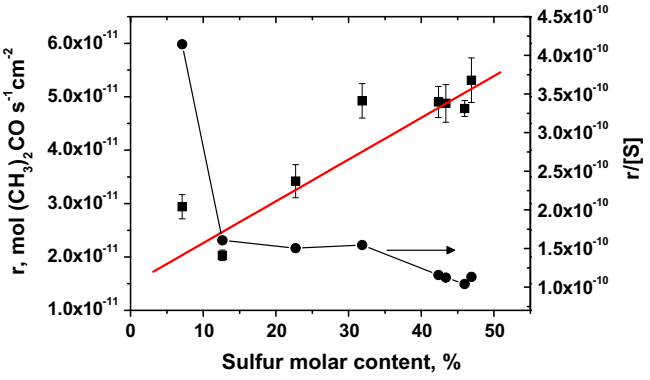


**Fig. 8.** Initial acetone formation rate (left ordinate) and initial acetone formation rate normalized to sulfur content (right ordinate) as a function of sulfur molar content in CdS catalysts. Isopropanol initial concentration 500 ppm, relative humidity 65%, reaction temperature 40 °C.

(10)). The equation does not take in account the effects of light scattering and reflection. By inserting all values in Eq. (6), we obtain the dependence of the rate on CdS fraction

$$r = I_0(1 - 10^{-48\chi_S}) \cdot \mathrm{LH}. \quad (7)$$

Thus, the rate of reaction should have reached 99% of its maximum value already at CdS content $\chi_S = 0.04$ according to Eq. (7). Fig. 8 demonstrates that the rate increases further when the fraction of CdS exceeds 10%. Normalization of the rate to the CdS fraction in catalysts shows linear proportionality between sulfur content and activity at higher sulfur contents in contradiction with Eq. (6). This discussion proves that the rate of isopropanol oxidation over catalysts containing CdS depends on CdS catalyst properties as a result of synthesis conditions changes and to a lower extent on CdS content.

Our results show that one-phase hexagonal CdS without impurities is the best photocatalyst for the isopropanol gas-phase oxidation. This contrasts with the earlier finding that the multi-phase composition CdS–$Cd(OH)_2$ of the photocatalysts can lead to higher activity due to the decrease in electron–hole recombination via charge separation [45]. The high photocatalytic activity could also be caused by the developed porous structure with hollow nanorods, advantageous for the photocatalytic reactions [20].

Another reason for increased photocatalytic activity of catalysts with stoichiometric S to Cd ratio can be associated with the quantum-size effect. Fig. 4A shows diffuse reflectance spectra of the samples with different S to Cd ratio. One can see that samples with

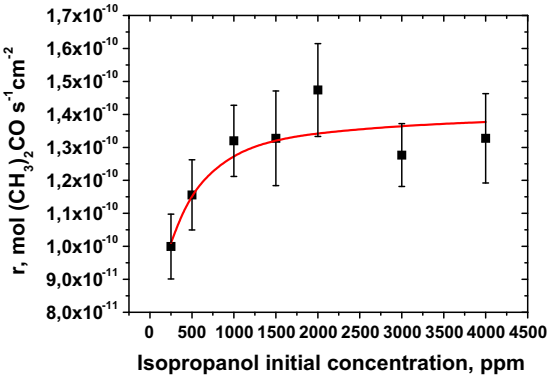


**Fig. 9.** Dependence of acetone formation initial rate on isopropanol initial concentration in the photocatalytic oxidation of isopropanol vapors and the L–H curve approximation. Relative humidity 65%, reaction temperature 40 °C. Catalyst #23.

increased sulfur content have the absorption threshold shifted toward the red part of the spectrum. Therefore, a larger part of the incident visible light is absorbed, and higher reaction rate can be attained at the same quantum yield.

Quantum efficiency for each catalyst of the above series were determined according to band gap energy obtained using diffuse reflectance spectroscopy. The following equation was used.

$$\varphi = \frac{r}{\Phi} \cdot 100\%, \quad (8)$$

where $\Phi$ – photon irradiance (mol $s^{-1}$ $cm^{-2}$), $\varphi$ – quantum efficiency and $r$ – acetone formation rate (mol $s^{-1}$ $cm^{-2}$). The quantum yields are given in Table 2. Quantum efficiency for one of the most active catalyst (#23) at isopropanol initial concentration 3000 ppm and relative humidity 65% was found to be 6.6% that is significantly higher compared to 2% demonstrated earlier by Green and Rudham for liquid-phase isopropanol photocatalytic oxidation on CdS [46].

### 3.3. Kinetic studies

Up to the present time, gas-phase photocatalytic oxidation has not been studied over CdS photocatalysts. Thus, it is highly interesting to learn how reaction conditions affect the reaction rate. The influence of isopropanol concentration, air humidity and reaction time was studied for isopropanol oxidation. The most active #23 catalyst was taken for the kinetic studies.

Fig. 9 shows how acetone formation rate depends on the isopropanol initial concentration. Since partial CdS catalyst deactivation is observed during oxidation, only initial three measurements during the initial 40 min of oxidation were taken and approximated with the following linear function was used to obtain the acetone formation initial rate at $t = 0$ moment.

$$r(t) = r_0 + A \cdot t, \quad (9)$$

where $r(t)$ – acetone formation rate, $t$ – time of reaction and $r_0$ – acetone formation initial rate.

One can see that the rate increases with the increase in isopropanol concentration and stays nearly the same above isopropanol concentration 1500 ppm. The obtained experimental data can be approximated using the Langmuir–Hinshelwood rate expression.

$$r = k_1 \cdot \frac{K \cdot C}{1 + K \cdot C}, \quad (10)$$

where $C$ is the isopropanol concentration, $k_1$ is the reaction rate constant and $K$ is the effective adsorption constant. The following constants were found by fitting the experimental points: $k_1 = 1.41 \times 10^{-10}$ mol $s^{-1}$ $cm^{-2}$, $K = 0.0101$ $ppm^{-1}$. Earlier Tasbihi et al. found $k_1 = 0.3–3.6 \times 10^{-10}$ mol $s^{-1}$ $cm^{-2}$ for isopropanol

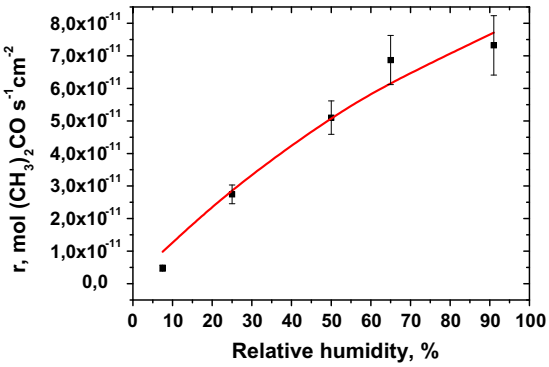


**Fig. 10.** Influence of relative humidity on acetone formation rate in the photocatalytic oxidation of isopropanol vapors. Photocatalyst #23, isopropanol initial concentration 500 ppm, reaction temperature 40 °C, halogen lamp IEK (150 W) with a cutoff filter ($\lambda \geqslant 410$ nm).

photocatalytic oxidation on $TiO_2$ under UV light [47]. The value of the constant is close to the value obtained earlier [47]. The higher value on $TiO_2$ was due to the fact that the authors used a xenon lamp that provided the light intensity practically 7-fold higher than in our experiments [47].

Adsorption of alcohols is the first stage of their photocatalytic oxidation. However, further mechanism of photocatalytic oxidation over CdS should be different from that over $TiO_2$ for the following reasons. Hydroxyl radicals are often supposed as active oxidizing species on UV irradiated $TiO_2$. However, the potential for the formation of hydroxyl radicals from water or less abundant hydroxyl anions is 2.6 and 1.8 V vs. NHE, respectively [48]. The valence band potential of CdS is about +1.7 V vs. NHE [49] as compared to +2.9 V for $TiO_2$ [49]. Therefore, the probability of hydroxyl radical formation on CdS is low. Direct reaction of organic species with photogenerated holes should be considered as the predominant way of oxidation on CdS.

The mechanism of oxygen involvement into the oxidation of organic species on CdS is not clear. The Mars–van Krevelen mechanism that is operational on $TiO_2$ [50] cannot be realized over CdS since oxygen cannot travel across the CdS lattice. Measurements of water content influence on oxidation rate can shed light on the oxidation mechanism.

Fig. 10 shows the influence of air humidity on photocatalytic oxidation rate of isopropanol. Unexpectedly, the rate increases strongly with an increase in reaction mixture humidity. The dependence can be described with Langmuir–Hinshelwood model that upon fitting gives parameters $k_1 = 2.0 \times 10^{-10}$ mol $s^{-1}$ $cm^{-2}$ and $K = 0.0068$ $(\%)^{-1}$. The increase in oxidation rate with the increase in humidity on CdS contrasts strongly with the effect of water vapor on photocatalytic oxidation over $TiO_2$. Earlier it was shown that $TiO_2$ catalyst activity in gas-phase isopropanol oxidation falls down with relative humidity increase [51].

This principal difference between CdS and $TiO_2$ should be associated with the different mechanism of photocatalytic oxidation. The increase in the rate with increase in humidity could be due to the larger amounts of hydroxyl radicals formed by reaction of water or hydroxide anions with photogenerated holes. However, as we demonstrated above, the formation of hydroxyl radicals should be very limited over CdS due to thermodynamical reasons and their supposed role should be minor. Organic compounds could be oxidized directly by photogenerated holes with the formation of the corresponding radical-cations.

$$RH + h^+ \rightarrow RH^+. \quad (11)$$

The radical-cations can further dissociate into organic radical and solvated proton.

$$RH^+ + H_2O \rightarrow R^{\cdot} + H_3O^+. \quad (12)$$

The stoichiometric surface of cadmium sulfide is not hydrated or populated with hydroxyl groups. Therefore, high water vapor concentrations in the gas phase should be needed in order to create the surface layer of adsorbed water, which dissolves the charged oxidation intermediates.

Another very important difference of CdS from $TiO_2$ is that Mars–van Krevelen mechanism with lattice transport of oxygen is not possible. Photogenerated holes and electrons tend to migrate and react over different crystallographic faces as has been demonstrated for $TiO_2$ [52]. If the distance between the faces for holes and electrons reactions is significant, then charged products have to travel toward each other in order to react and form the final uncharged products. In the case of $TiO_2$, reduced oxygen $O^{2-}$ can travel across the lattice to the needed places as a consequence of photoexcitation. For CdS, such transport through the lattice is not possible. Nor is it possible via surface diffusion because the CdS surface is generally of low polarity. The surface layer of adsorbed water on CdS can play the role of the transport medium for charged oxygen species forming during electrons capture.

$$O_2 + e^- \rightarrow O_2^{\cdot-}, \quad (13)$$

$$O_2^{\cdot-} + H_2O \rightleftarrows HO_2^{\cdot} + OH^-, \quad (14)$$

$$OH^- + H_3O^+ \rightleftarrows 2H_2O. \quad (15)$$

The overall reaction mechanism for photocatalytic oxidation of isopropanol over CdS proceeds via the following stages. At first, light absorption by semiconductor particles occurs producing conduction band electrons and valence band holes (Eq. (16)). The holes and electrons may migrate to the surface of catalyst (Eqs. (17) and (18)) or recombine with each other (19). Water molecules can be needed for the transport of charged species forming from oxygen (Eqs. (20)–(22)). It was revealed by Davis et al. [27, 28] that reaction between surface holes and adsorbed organics is the main way for cadmium sulfide to oxidize organics (Eq. (25)). The final product of oxidation, acetone, is formed as a result of electron injection from radical $(CH_3)_2COH$ into CdS (26).

$$CdS \xrightarrow{h\nu} CdS(h^+ + e^-), \quad (16)$$

$$h^+ \rightarrow h^+_{surf}, \quad (17)$$

$$e^- \rightarrow e^-_{surf}, \quad (18)$$

$$h^+ + e^- \rightarrow \text{recombination}, \quad (19)$$

$$e^-_{surf} + O_2 \rightarrow O_2^{\cdot-}, \quad (20)$$

$$O_2^{\cdot-} + H^+ \rightarrow HO_2^{\cdot}, \quad (21)$$

$$HO_2^{\cdot} + e^-_{surf} \rightarrow HO_2^{\cdot-}, \quad (22)$$

$$HO_2^- + H^+ \rightarrow H_2O_2, \quad (23)$$

$$H_2O_2 + 2e^-_{surf} + 2H^+ = 2H_2O, \quad (24)$$

$$(CH_3)_2CHOH + h^+_{surf} \rightarrow (CH_3)_2C^{\cdot}OH + H^+, \quad (25)$$

$$(CH_3)_2C^{\cdot}OH + CdS \rightarrow (CH_3)_2CO + H^+ + CdS(e^-). \quad (26)$$

The presence of $H_2O$ layer on CdS surface can also be important for the stabilization of radicals formed as intermediates during the oxidation reaction stages and making them more favorable

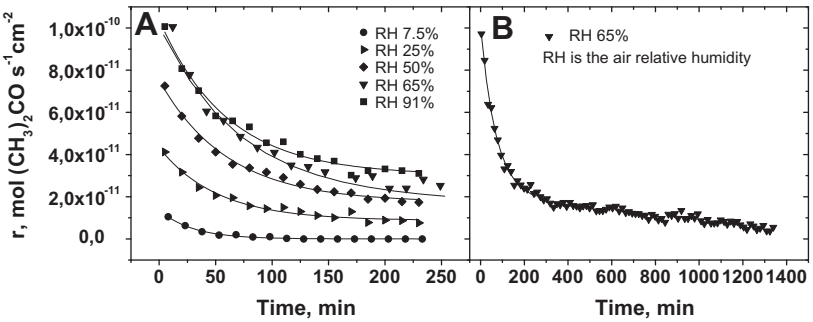


**Fig. 11.** Dependence of acetone formation rate on time on stream at various RH during 230 min (A) and at 65% RH during 1350 min (B). Photocatalyst #23, isopropanol initial concentration 500 ppm, reaction temperature 40 °C, halogen lamp IEK (150 W) with a cutoff filter ($\lambda \geqslant 410$ nm).

thermodynamically. Radicals can be very unstable in a gas phase, so water molecules can help them to survive. Thus, $H_2O$ molecules take a very important part in both oxidation on $TiO_2$ and CdS.

Vildozo et al. has reported for PCO of isopropanol vapors on $TiO_2$ that relative humidity increase leads to the adsorption competition between water and organic compound [51]. This fact is explained by extremely high $TiO_2$ surface hydrophilic properties. Cadmium sulfide is not as hydrophilic compound as titanium dioxide. CdS catalyst surface probably has not enough ability to adsorb large amounts of water vapors that correspond to competition for adsorption sites. So isopropanol vapor oxidation rate on CdS increases with relative humidity increase continuously. Isopropanol molecules can be absorbed by the surface water layer on CdS surface, and this layer could increase the surface concentration of isopropanol.

It is well known that a typical problem of using cadmium sulfide as the photocatalyst in solutions is deactivation due to its photocorrosion. Therefore, it is very interesting to examine photocatalytic oxidation on CdS in gas phase. The flow-type reactor used allows one to measure both the reaction rate and the stability of the photocatalyst. Fig. 11A demonstrates the temporal profiles of activity at different RH. One can see that activity decreases with reaction time at any RH used. However, the deactivation time and the residual activity increase as RH grows. The obtained experimental profiles were approximated using the single exponential decay.

$$r = r_0 + A \cdot e^{-\frac{t}{\tau}}, \tag{27}$$

where $r$ – the acetone formation rate (mol $s^{-1}$ $cm^{-2}$), $t$ – the reaction time (min), $r_0$ – the steady acetone formation rate, $A$ – the rate decrease during deactivation and $\tau$ – the characteristic time of catalyst deactivation. The results of data fitting are shown in Table 3.

One can see that relative humidity growth from 7.5% to 25% allows increasing deactivation characteristic time from 29 to 60 min. The residual activity after the deactivation, $r_0$, increases continuously from zero at low RH to a significant value at RH 91%. A possible reason for the positive influence of humidity on photocatalytic oxidation over CdS is that the film of adsorbed water dissolves compounds causing deactivation and frees the CdS surface.

Fig. 11B shows the typical dependence of the acetone formation rate on the reaction time for the most active obtained catalyst #23 over a long reaction period at RH 65%. One can see that the gradual deactivation of the catalyst occurred, but the activity is not lost completely. The deactivation process can be described by the exponential decay combined with a linear decrease.

$$r = 2.39 \times 10^{-11} + 9.07 \times 10^{-11} \cdot e^{-\frac{t}{55.37}} - 1.516 \times 10^{-14} \cdot t, \tag{28}$$

where $r$ is the acetone formation rate (mol $s^{-1}$ $cm^{-2}$) and $t$ is the reaction time (min). The characteristic time of activity decay is 55.3 min. After the exponential period, the activity declines slowly in a linear manner. It is interesting that activity is not lost completely: even after 22 h of reaction, the oxidation rate was $4.8 \times 10^{-12}$ mol $s^{-1}$ $cm^{-2}$.

**Table 3**
Characteristic parameters of deactivation curves approximation for different relative humidity.

| Relative humidity (%) | $r_0$ (mol/(s $cm^2$)) | $A$ (mol/(s $cm^2$)) | $\tau$ (min) |
|---|---|---|---|
| 7.5 | 0 | $1.37 \times 10^{-11}$ | 29.14 |
| 25 | $7.56 \times 10^{-12}$ | $3.46 \times 10^{-11}$ | 58.41 |
| 50 | $1.74 \times 10^{-11}$ | $5.78 \times 10^{-11}$ | 60.59 |
| 65 | $2.39 \times 10^{-11}$ | $9.07 \times 10^{-11}$ | 55.37 |
| 91 | $3.03 \times 10^{-11}$ | $7.37 \times 10^{-11}$ | 60.23 |

In order to identify the surface changes that cause catalyst deactivation, XPS research was performed. Fig. 12 demonstrates Cd*3d* and S*2p* spectra of fresh and deactivated CdS catalyst #23 that have operated at 65% RH during 1350 min (see Fig. 11B). Cd*3d* peak can be described as a doublet $Cd3d_{5/2}$–$Cd3d_{3/2}$ with integral intensity ratio 3:2 and spin–orbit energy shift 6.73 eV. Binding energy of $Cd3d_{5/2}$ is 405.2 eV that corresponds to cadmium cations in CdS [53–55]. In S*2p* spectra of fresh catalyst, one can observe a doublet $S2p_{3/2}$–$S2p_{1/2}$ with integral intensity ratio 2:1 and spin–orbit energy shift 1.18 eV. Binding energy of $S2p_{3/2}$ is 161.7 eV, which also conforms to sulfur in CdS [53–55]. In S2p spectra of deactivated catalyst, one can see additional doublet with a substantially higher binding energy $E_B(S2p_{3/2})$ = 168.1 eV, which corresponds to sulfate groups $SO_4^{2-}$ [56]. Furthermore, increase in line intensity with binding energy 531.6 eV is observed in O1*s* spectra (not shown in Fig. 12). Moreover, the ratio of oxygen O1*s* to sulfur $S2p_{3/2}$ amount is 3.9:1. All of these facts allow us to suggest that the second doublet in deactivated catalyst spectra corresponds to sulfur in $SO_4^{2-}$ group. The formation of sulfate and cadmium (II) in aqueous solution was previously observed during photooxidative CdS dissolution [57]. XRD investigations of the spent catalyst (not shown) did not reveal any changes in the bulk semiconductor phase composition.

The mechanism of sulfate formation has been proposed previously by Meissner [58] and includes formation of photogenerated charge carriers

$$CdS + h\nu \rightarrow CdS(e^- + h^+); \tag{29}$$

oxidation of sulfide with photogenerated holes

$$CdS + 2h^+ \rightarrow Cd^{2+} + S; \tag{30}$$

reduction of oxygen with photogenerated electrons

$$O_2 + e^- \rightarrow O_2^-; \tag{31}$$

and reaction of oxygen radical anions with sulfur

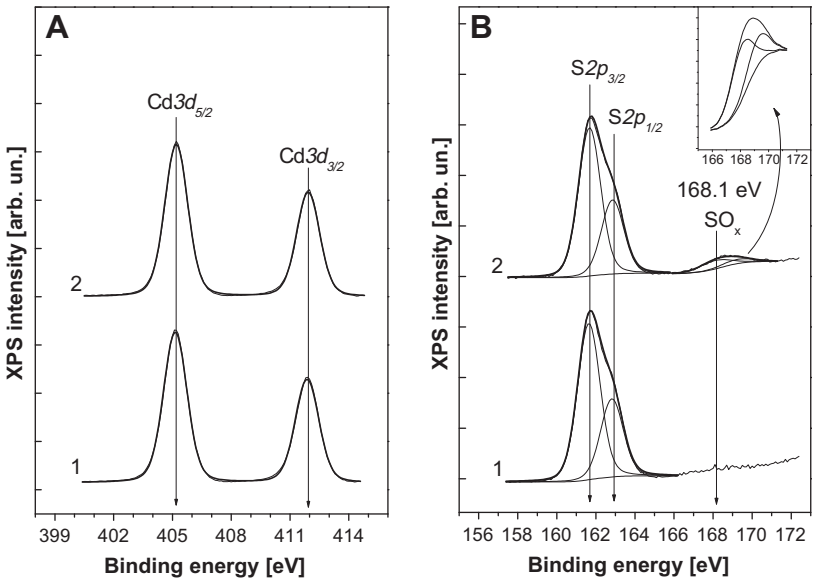


**Fig. 12.** XPS spectra of fresh (1) and deactivated (2) CdS catalyst. Picture (a) demonstrates Cd3*d* spectra, and picture (b) shows S2*p* spectra.

$$S + 2O_2^- \rightarrow SO_4^{2-}. \quad (32)$$

Photodissolution with the formation of $SO_4^{2-}$ and $Cd^{2+}$ leads to the destruction of the CdS photocatalyst [24]. In our case, formation of sulfate species results in the deactivation of CdS photocatalyst for gas-phase alcohols oxidation. The sulfate anions cover CdS surface and hinder oxidation and reduction reactions between holes, electrons and reagents. Higher amounts of water help to keep the reaction steady by dissolving sulfates.

## 4. Conclusions

The results distinctly demonstrate that the two-step synthesis method allows obtaining CdS catalyst with high photocatalytic activity in gas-phase ethanol and isopropanol oxidation reactions. The most efficient conditions of synthesis are found to be high stirring rate and slow reagents addition rate. Catalysts activity grows with the S to Cd molar ratio increase in precursor solutions and reaches its maximum value at 2:1. XRD and XRF measurements reveal that the catalyst obtained with 2:1 sulfur to cadmium molar ratio contains the highest sulfur amount that is close to the stoichiometric ratio in CdS. Alcohol vapors' photocatalytic oxidation under visible light irradiation was carried out in a batch and in a flow-type reactors. Langmuir–Hinshelwood rate expression was used to describe PCO kinetic features, and appropriate constants were found. The CdS is deactivated in alcohol vapors oxidation, but the increase in air humidity leads to lower deactivation effects. It was established that the photooxidation rate increases with the relative humidity rise. Photocatalyst deactivation was investigated. XPS measurements showed that the catalyst deactivation is accompanied by the oxidation of surface $S^{2-}$ into $SO_4^{2-}$.

## Acknowledgements

We gratefully acknowledge the support of the Federal Special Program "Scientific and Educational Cadres of Innovative Russia" (2009–2013 years) via Contract P1360, SB RAS Integration Projects 70 and 36, Presidium RAS Grant 27.56 as well as the Ministry of education and science of Russia via Contract 16.513.11.3091. We thank Drs. S.V. Cherepanova, V.V. Kaichev and A.V. Miller for the help with obtaining and treating spectral data.

## References

[1] J.T. Carneiro, C.C. Yang, J.A. Moulijn, G. Mul, J. Catal. 277 (2011) 129.
[2] S. Higashimoto, N. Suetsugu, M. Azuma, H. Ohue, Y. Sakata, J. Catal. 274 (2010) 76.
[3] Y. Shiraishi, M. Ikeda, D. Tsukamoto, S. Tanaka, T. Hirai, Chem. Comm. 47 (2011) 4811.
[4] L. Pan, J.J. Zou, X.W. Zhang, L. Wang, Ind. Eng. Chem. Res. 49 (2010) 8526.
[5] K. Ikeue, S. Nozaki, M. Ogawa, M. Anpo, Catal. Today 74 (2002) 241.
[6] K. Koci, L. Obalova, L. Matejova, D. Placha, Z. Lacny, J. Jirkovsky, O. Solcova, Appl. Catal. B: Environ. 89 (2009) 494.
[7] L.N. Protasova, E.V. Rebrov, T.S. Glazneva, A. Berenguer-Murcia, Z.R. Ismagilov, J.C. Schouten, J. Catal. 271 (2010) 161.
[8] G.L. Chiarello, M.H. Aguirre, E. Selli, J. Catal. 273 (2010) 182.
[9] O.S. Mohamed, A.E.-A.M. Gaber, A.A. Abdel-Wahab, J. Photochem. Photobiol. A: Chem. 148 (2002) 205.
[10] S. Higashimoto, N. Suetsugu, M. Azuma, H. Ohue, Y. Sakata, J. Catal. 274 (2010) 76.
[11] J.T. Carneiro, J.A. Moulijn, G. Mul, J. Catal. 273 (2010) 199.
[12] J.T. Carneiro, Ch.-Ch. Yang, J.A. Moulijn, G. Mul, J. Catal. 277 (2011) 129.
[13] J.S. Jang, Ch.-J. Yu, S.H. Choi, S.M. Ji, E.S. Kim, J.S. Lee, J. Catal. 254 (2008) 144.
[14] Y. Fan, M. Deng, G. Chen, Q. Zhang, Y. Luo, D. Li, Q. Meng, J. Alloy Compd. 509 (2011) 1477.
[15] K. Kalyanasundaram, E. Borgarello, D. Duonghong, M. Graetzel, Angew. Chem. Int. Ed. 20 (1981) 987.
[16] X. Zong, H.J. Yan, G.P. Wu, G.J. Ma, F.Y. Wen, L. Wang, C. Li, J. Am. Chem. Soc. 130 (2008) 7176.
[17] X.W. Wang, G. Liu, Z.G. Chen, F. Li, L.Z. Wang, G.Q. Lu, H.M. Cheng, Chem. Commun. (2009) 3452.
[18] W.Z. Tang, C.P. Huang, Chemosphere 30 (1995) 1385.
[19] G. Lin, J. Zheng, R. Xu, J. Phys. Chem. C 112 (2008) 7363.
[20] N.Z. Bao, L.M. Shen, T. Takata, K. Domen, Chem. Mater. 20 (2008) 110.
[21] Y. Huang, F. Sun, T. Wua, Q. Wua, Z. Huang, H. Su, Z. Zhang, J. Solid State Chem. 184 (2011) 644.
[22] Y. Yu, Y. Ding, S. Zuo, J. Liu, Int. J. Photoenergy (2011) 762929.
[23] L. Nguyena, R. Khoa, W. Baec, R.K. Mehra, Chemosphere 38 (1999) 155.
[24] A.P. Davis, C.P. Huang, Langmuir 7 (1991) 709.
[25] C. Karunakaran, S. Senthilvelan, Sol. Energy 79 (2005) 505.
[26] K.V.S. Rao, B. Srinivas, A.R. Prasad, M. Subrahmanyam, Chem. Comm. (2000) 1533.
[27] B. Ohtani, J. Kawaguchi, M. Kozawa, S. Nishimoto, T. Inui, J. Chem. Soc. Faraday Trans. 91 (1995) 1103.
[28] B. Ohtani, S. Kusakabe, K. Okada, S. Tsuru, S. Nishimoto, Y. Amino, K. Izawa, Y. Nakato, M. Matsumura, Y. Nakaoka, Y. Nosaka, J. Chem. Soc., Perkin Trans. 2 (2001) 201.
[29] A. Maldotti, L. Andreotti, A. Molinari, S. Tollari, A. Penobi, S. Cenini, J. Photochem. Photobiol. A 133 (2000) 129.
[30] B. Huang, Y. Yang, X. Chen, D. Ye, Catal. Commun. 11 (2010) 844.
[31] S. Biswas, M.F. Hossain, T. Takahashi, Y. Kubota, A. Fujishima, Phys. Status Solidi A 205 (2008) 2028.
[32] M. Fujii, K. Nagasuna, M. Fujishima, T. Akita, H. Tada, J. Phys. Chem. C 113 (2009) 16711.
[33] W. Zhang, R. Xu, Int. J. Hydrogen Energy 34 (2009) 8495.

[34] K. Zhang, D. Jing, C. Xing, L. Guo, Int. J. Hydrogen Energy 32 (2007) 4685.
[35] S. Biswas, S. Kar, S. Santra, Y. Jompol, M. Arif, S.I. Khondaker, J. Phys. Chem. C 113 (2009) 3617.
[36] X. Fan, M.L. Zhang, I. Shafiq, W.J. Zhang, C.S. Lee, S.T. Lee, Cryst. Growth Des. 9 (2009) 1375.
[37] S. Acharya, I. Patla, J. Kost, S. Efrima, Y. Golan, J. Am. Chem. Soc. 128 (2006) 9294.
[38] E.A. Kozlova, T.P. Lyubina, M.A. Nasalevich, A.V. Vorontsov, A.V. Miller, V.V. Kaichev, V.N. Parmon, Catal. Commun. 12 (2011) 597.
[39] S. Cherepanova, S. Tsybulya, Mater. Sci. Forum 443–444 (2004) 87–90.
[40] R.T. Downs, K.L. Bartelmehs, G.V. Gibbs, M.B. Boisen, Am. Mineral. 78 (1993) 1104.
[41] X. Xu, R. Lu, X. Zhao, S. Xu, X. Lei, F. Zhang, D.G. Evans, Appl. Catal. B 102 (2011) 147.
[42] M.B. Ortuno-Lopez, M. Sotelo-Lerma, A. Mendoza-Galvan, R. Ramırez-Bon, Thin Solid Films 457 (2004) 278.
[43] D.V. Bavykin, Luminescent Properties of Cadmium Sulfide Nanocolloids, Phd Thesis, Novosibirsk, 1998, p. 11.
[44] K. Senthil, D. Mangalaraj, Sa.K. Narayandass, B. Hong, Y. Roh, C.S. Park, J. Yi, Semicond. Sci. Technol. 17 (2002) 97.
[45] J. Zhensheng, L. Qinglin, F. Liangbo, Ch. Zhengshi, Zh. Xinhua, X. Chanjuan, J. Mol. Catal. 50 (1989) 315.
[46] K.J. Green, R. Rudham, J. Chem. Soc. Faraday Trans. 88 (1992) 3599.
[47] M. Tasbihi, U.L. Štangar, A.S. Škapin, A. Ristić, V. Kaučič, N.N. Tušar, J. Photochem. Photobiol. A 216 (2010) 167.
[48] G.V. Buxton, C.L. Greenstock, W.P. Helman, A.B. Ross, J. Phys. Chem. Ref. Data 17 (2) (1988).
[49] L. Palmisano, A. Sclafani, in: M. Schiavello (Ed.), Wiley Series in Photoscience and Photoengineering, vol. 3, England, 1997.
[50] A.R. Almeida, J.A. Moulijn, G. Mul, J. Phys. Chem. C 115 (2011) 1330.
[51] D. Vildozo, C. Ferronato, M. Sleiman, J.-M. Chovelon, Appl. Catal. B 94 (2010) 303.
[52] T. Ohno, K. Sarukawa, M. Matsumura, New J. Chem. 26 (2002) 1167.
[53] C.J. Vesely, D.W. Langer, Phys. Rev. B 4 (1971) 451.
[54] M. Stoev, A. Katerski, J. Mater. Chem. 6 (1996) 377.
[55] G. Hota, S.B. Idage, K.C. Khilar, Colloids Surf. A 293 (2007) 5.
[56] D. Briggs, G. Beamson, Anal. Chem. 64 (1992) 1729.
[57] Y.H. Hsieh, C.P. Huang, Coll. Surf. 53 (1991) 275.
[58] D. Meissner, R. Memming, L. Shuben, S. Yesodharan, M. Graetzel, Ber. Bunsenges. Phys. Chem. 89 (1985) 121.